# PCCP

## Accepted Manuscript

This is an *Accepted Manuscript*, which has been through the Royal Society of Chemistry peer review process and has been accepted for publication.

*Accepted Manuscripts* are published online shortly after acceptance, before technical editing, formatting and proof reading. Using this free service, authors can make their results available to the community, in citable form, before we publish the edited article. We will replace this *Accepted Manuscript* with the edited and formatted *Advance Article* as soon as it is available.

You can find more information about *Accepted Manuscripts* in the Information for Authors.

Please note that technical editing may introduce minor changes to the text and/or graphics, which may alter content. The journal's standard Terms & Conditions and the Ethical guidelines still apply. In no event shall the Royal Society of Chemistry be held responsible for any errors or omissions in this *Accepted Manuscript* or any consequences arising from the use of any information it contains.

# High intrinsic carrier mobility and photon absorption in perovskite CH$_3$NH$_3$PbI$_3$

Youwei Wang,[1] Yubo Zhang,[1] Peihong Zhang,[2] Wenqing Zhang[1,3*]

[1]*State Key Laboratory of High Performance Ceramics and Superfine Microstructures, Shanghai Institute of Ceramics, Chinese Academy of Sciences, Shanghai 200050, China*

[2]*Department of Physics, University at Buffalo, SUNY, Buffalo, New York 14260, USA*

[3]*Materials Genome Institute, Shanghai University, Shanghai 200444, China*

### Abstract

The carrier transport and optical properties of the hybrid organic-inorganic perovskite CH$_3$NH$_3$PbI$_3$ are investigated using first-principles approaches. We found that electron and hole mobilities could reach surprisingly high values of $(7 \sim 30) \times 10^3$ and $(1.5 \sim 5.5) \times 10^3$ cm$^2$/V·s, respectively, and the both are estimated to be much higher than the current experimental measurements. The high carrier mobility is ascribed to the intrinsically small effective masses of anti-bonding band-edge states. The above results imply that there is still space to improve the performance of related solar cells. This material also has sharp photon absorption edge and absorption coefficient as high as $10^5$ cm$^{-1}$, both of which contribute to effective utilization of solar radiation. Although band-edge states are mainly derived from the inorganic ions of Pb and I, the thermal movement of organic base has indirect influences on the bandgap and carrier effective masses, resulting in the temperature-dependent solar cell efficiencies.

## 1. Introduction

Dye-sensitized solar cell is considered to be one of the most promising third-generation photovoltaic cells, owing to their high efficiency, low cost, and simple printing fabrication process. Although the related researches date back to the 1920s,[1] the cell efficiency was below 12% for a long time.[2,3] Recently, a major breakthrough is achieved in the organic-inorganic hybrid solar cells, i.e., the emerging methylammonium lead iodide (CH$_3$NH$_3$PbI$_3$) with perovskite structure.[4-8] The cell efficiency is as high as 19.3%,[9] which is comparable to the best record of 20.3% for the Cu(In,Ga)Se$_2$ cell.[10] Such a high cell efficiency is ascribed to the long diffusion length[6,7] and the large absorption coefficient.[11]

Considerable efforts have been devoted to the microscopic mechanism of the superior performance in the fundamental research community. For example, first-principles investigations found that the separation of electron-hole pair can be effectively assisted by the spontaneous electric polarization in these hybrid materials, which is induced by the organic base.[12] It was also found that the carrier diffusion length can be affected by the unusual defect properties, which is strongly correlated with the anti-bonding coupling between Pb-6$s$ and I-5$p$ states at the valence band maximum (VBM).[13] Experimental research showed that the electron-hole diffusion length in mixed halide CH$_3$NH$_3$PbI$_{3-x}$Cl$_x$ is around one micrometer, one order of magnitude greater than its absorption length.[6] Such long diffusion length is beneficial for the effective separation and collection of the photon-excited carriers. Generally speaking, the extremely long diffusion length should imply high carrier mobility and/or low recombination rate of the electron-hole pairs. However, the measured electron mobility is only 66 cm$^2$/V·s for perovskite CH$_3$NH$_3$PbI$_3$, which is rather smaller than expected, compared with 2320 cm$^2$/V·s in CH$_3$NH$_3$SnI$_3$.[14]

Earlier experiments also confirmed that the absorption coefficient of CH$_3$NH$_3$PbI$_3$ is as high as $10^5$ cm$^{-1}$, which is comparable to those of GaAs and Cu(In,Ga)Se$_2$.[11] The high absorption coefficient explains the reason that

*Corresponding E-mail address: wqzhang@mail.sic.ac.cn

thin absorber films can suffice for practical perovskite solar cells.[4,5] Indeed, the observed high photoluminescence quenching (>90%) is a strong manifestation of efficient charge transfer from $CH_3NH_3PbI_3$ to $PC_{61}BM$ (abbreviation for [6,6]-phenyl-$C_{61}$-butyric acid methyl ester) at the interface.[15] Moreover, the optical bandgap of 1.5 eV also ensures an optimal utilization of the solar spectral irradiance for a single junction solar cell.[16]

In this work, we investigated the carrier transport properties using approaches based on the deformation potential theory.[17] Furthermore, we also calculated the optical absorption coefficient. The intrinsic carrier mobility and photon absorption are found to be rather high in perovskite $CH_3NH_3PbI_3$, which partly explains why the solar cells can achieve such high efficiencies. Finally, we discussed the indirect influence of thermal movement of the organic base on the transport and optical properties by tuning the Pb-I framework. That effect of organic base leads to temperature-dependent solar cell efficiencies.

## 2. Computational details

The structural and electronic properties are investigated using the plane-wave projector-augmented wave method[18,19] as implemented in the Vienna *ab initio* simulation (VASP) package.[20,21] We employed 4×4×4 Monkhorst-pack *k*-meshes[22] for structural relaxation and electronic properties calculations. For structural relaxation, we used the van der Waals density functional (vdW-DF)[23] in the form of optB86b-vdW[24] to calculate the dispersion interaction between the organic base and the Pb-I framework. The electronic properties are comparatively investigated by using the Perdew-Burke-Ernzerh (PBE)[25] functional and the modified Becke-Johnson (mBJ) potential.[26-29] Because near-edge states contains considerable heavy *p*-electrons from the Pb and I elements, the spin-orbit coupling (SOC) effect is taken into consideration. Starting from the above obtained band structures, we further investigated the carrier transport and optical properties. The carrier mobility is calculated using deformation potential theory.[17] Optical absorption properties[30] are calculated using the independent particle approximation as implemented in the all-electron WIEN2k code[31] with much denser 20×20×20 *k*-meshes.

## 3. Results and discussion

### 3.1. A brief introduction to the structural properties

Before presenting the results, we first introduced the structural properties of three phases of $CH_3NH_3PbI_3$. Whereas the Pb-I octahedra forms the framework of perovskite, the large organic base $CH_3NH_3^+$ (i.e., the A-site cation in the standard $ABO_3$ perovskite) occupies the void formed by adjacent octahedra. The organic base interacts with the Pb-I inorganic framework through the dispersion interaction between methyl and iodide ions. Because the vdW force is relatively weak, such bonding can be easily destroyed by, for example, temperature effect. As a result, $CH_3NH_3PbI_3$ transits from orthorhombic phase to tetragonal phase at 161.4 K, and further to cubic phase at 330.4 K,[32] which is mainly due to the strong dynamic movement of the organic base. The primitive cells have 48, 48, and 12 atoms for the orthorhombic ($a = 8.490$, $b = 8.948$, $c = 12.556$ Å), tetragonal ($a = b = 8.851$, $c = 12.444$ Å), and cubic ($a = b = c = 6.276$ Å) phases, respectively. In order to make a straight-forward comparison of the three systems, we reconstructed the cubic structure by doubling the lattice $c$ (i.e., $c' = 2c$) to reflect similar symmetry with the orthorhombic and tetragonal counterparts and the resulting structure ($a' = b' = c'/\sqrt{2} = 8.876$ Å) is taken as "pseudo-cubic" phase, presenting the orientations of organic base different but keeping the sub-lattice of Pb-I framework cubic phase.

Experimentally, the orientations of the organic base in the high-temperature tetragonal and cubic structures cannot be well resolved due to the thermal movement of the organic base. In our work, the theoretical crystal structures are obtained by optimizing ion positions with lattice parameters fixed to the experimentally values. As a result, the thermal movement (or orientational disorder) effect of organic base is partially considered in our structures. In other words, the simple approximation to the crystal structure is inadequate to fully explore the thermal movement effect and thus the detailed influences on the carrier transport and optical properties. However, we argued that the transport and optical properties are mainly determined by the Pb-I interactions. And the thermal movement effect will be briefly discussed below.

### 3.2. High mobilities of electrons and holes

Whereas a similar system of $CH_3NH_3SnI_3$ was reported to have a high electron mobility ($\mu_e$ ~2320 cm$^2$/V·s) from experimental measurement, the electron mobility ($\mu_e$ ~66 cm$^2$/V·s) seems too small for $CH_3NH_3PbI_3$.[14] In this work, the transport properties are evaluated using a simple approach based on the deformation potential theory as shown bellow[17]:

$$\mu = \frac{(8\pi)^{\frac{1}{2}}\hbar^4 e c_{ii}}{3\left(m^*\right)^{\frac{5}{2}}(k_B T)^{\frac{3}{2}} E_1^2},$$

where $\hbar$ is the reduced Planck constant, $e$ is the element charge, $c_{ii}$ is the elastic constant, $m^*$ is the effective mass of charge, $k_B$ is the Boltzmann constant, $T$ is the temperature, and $E_1$ is the deformation potential.[33-35] The deformation potential ($E_1$) is defined as energy shift of the band energy position ($\Delta E$) with respect to a small lattice dilation ($\Delta l$) along a lattice ($l_0$) direction, i.e., $E_1 = \Delta E/(\Delta l/l_0)$. It should be noticed that reliable band structures are highly essential for the calculations of carrier mobilities. In our calculations, the mBJ potential is employed with the SOC effect considered (see the Supplementary material) and the core levels are aligned to determine the energy shift of band-edge states.[34] The calculated carrier mobility, together with the deformation potential, elastic constant, and effective mass, are collected in Table I for the three phases.

Table I. Calculated deformation potential ($E_{1c}$ and $E_{1v}$ for electron and hole, respectively), elastic constant ($c_{ii}$), effective mass ($m_e$ and $m_h$ for electron and hole, respectively), and carrier mobility ($\mu_e$ and $\mu_h$ for electron and hole, respectively) at the $\Gamma$-point of the Brillouin Zone. Two directions are considered for the orthorhombic and tetragonal phases, and only one direction is calculated for the pseudo-cubic phase. Room temperature ($T=300 K$) is used in the calculation.

| | Orthorhombic | | Tetragonal | | Pseudo-cubic |
|---|---|---|---|---|---|
| | <001> | <100> | <001> | <100> | <001> |
| $E_{1c}$ (eV) | −4.89 | −1.49 | −4.40 | −1.48 | −4.41 |
| $E_{1v}$ (eV) | −6.74 | −4.05 | −6.41 | −3.26 | −7.77 |
| $c_{ii}$ (kBar) | 443 | 267 | 423 | 233 | 396 |
| $m_e$ ($m_0$) | 0.18 | 0.26 | 0.21 | 0.24 | 0.11 |
| $m_h$ ($m_0$) | 0.27 | 0.30 | 0.28 | 0.31 | 0.14 |
| $\mu_e$ ($10^3$cm$^2$/V·s) | 8.30 | 21.6 | 6.70 | 23.4 | 31.5 |
| $\mu_h$ ($10^3$cm$^2$/V·s) | 1.60 | 2.00 | 1.50 | 2.50 | 5.50 |

The calculated electron mobilities are around $(7 \sim 30) \times 10^3$ cm$^2$/V·s for the three phases, substantially higher than the experimentally measured data (experimental result of hole mobility is unavailable).[14] Our results are consistent with another recent theoretical work,[36] which predicted high carrier mobilities to be 3100 ~ 1500 cm$^2$/V·s for electrons and 1500~ 800 cm$^2$/V·s for holes from a simplified Kane model[37] with empirical parameters of the concentration varying from $10^{16}$ to $10^{19}$ cm$^{-3}$. The high mobilities for both the electron and hole are due to the small effective masses (see Table I), which can be inferred from the calculated band structure (see Fig. 2). Both the valence and conduction band-edge states are from the inorganic Pb-I framework, with the organic base only contributing to low energy bands (see Supplementary materials). The conduction band minimum (CBM) is composed of the Pb-6$p$ (amount to 80%) and I-5$p$ (20%) states, and the anti-bonding interaction results in rather small effective electron mass as usually found in simple semiconductors. The VBM is mainly from the I-5$p$ (70%), but also with some Pb-6$s$ (30%) states. Moreover, it should be noticed that the Pb-6$s$ states near the VBM are from the anti-bonding part of Pb-6$s^2$ lone pair,[13] with the bonding states around −7.5 eV from the VBM. As a result, the anti-bonding interaction at the VBM also results in small effective masses for the holes, comparable with that of the electrons.

The calculated hole mobilities in $CH_3NH_3PbI_3$ are lower than that of electrons, consistent with the usual

findings in simple semiconductors.[17] Generally speaking, the lower mobilities for the holes than the electrons in simple semiconductors are usually due to the heavier effective masses for the holes. However, the effective masses of electrons and holes are comparable in $CH_3NH_3PbI_3$ (see Table I). In fact, the main difference between electron and hole mobilities in $CH_3NH_3PbI_3$ derives from the deformation potential (~2 times higher for the holes than for the electrons), rather than from the effective masses as found in simple semiconductors, like Silicon. We analyzed this '*abnormal behavior*' of deformation potential in $CH_3NH_3PbI_3$ by investigating the band-edge electronic properties. Upon volume dilation, the site energy of the VBM is influenced by three factors (see Supplementary materials): (a) the decreasing of the kinetic energy, (b) the decreasing due to the Pb-6$s$ and I-5$p$ anti-bonding interaction, and (c) the negligibly increasing due to the small proportion of Pb-6$p$ and I-5$p$ bonding interaction. The CBM is influenced by two factors: (a) the decreasing of kinetic energy and (b) the decreasing due to Pb-6$p$ and I-5$p$ anti-bonding interaction. From Table I, it is obvious that the VBM site energy is more prone to change upon dilation than the CBM. In this regard, the anti-bonding interaction between Pb-6$s$ and I-5$p$ plays a major role in determining the site energy of the VBM. Since the deformation potential is a measure of the coupling strength of the carrier to acoustic phonon,[38] the phonon scattering is more severe for the hole than for electron in $CH_3NH_3PbI_3$. As a result, the hole has much lower mobility than the electron, despite that the hole and electron have quite similar effective masses at the band-edge states.

### 3.3. High optical absorption coefficient

In addition to the carrier mobility, we also evaluated absorption coefficients of $CH_3NH_3PbI_3$, which is another important factor to influence the solar cell efficiency (see Fig. 1). Generally speaking, the calculated spectra agree well with experimental results, especially that the peak near 2.5 eV from the measurement is well reproduced in the theoretical calculations (around 2.25 eV). However, the calculated absorption coefficient is slightly lower than the experimental results,[11] because the excitonic effect, quadrupole transition, and vibronic coupling effect are neglected in our calculations.

Two favorable factors contributing to the solar cell application can be easily confirmed from the spectra. First, the spectra show sharp shoulders near absorption edges, which is conducive to effective utilization of low-energy photons. Second, the absorption coefficients are as high as $10^4 \sim 10^5$ cm$^{-1}$ near the edges. The high absorption ability is due to the absorption between the I-5$p$ valence states and the Pb-6$p$ conduction states, both of which have high density of states. It is also benefited by the optical transition from the Pb-6$s$ states near the VBM to the Pb-6$p$ states near the CBM. So, while $CH_3NH_3PbI_3$ has comparable absorption ability to the well-known Cu(In,Ga)Se$_2$ material, $CH_3NH_3PbI_3$ has much sharper absorption edge and thus can better utilize the low-energy photons.
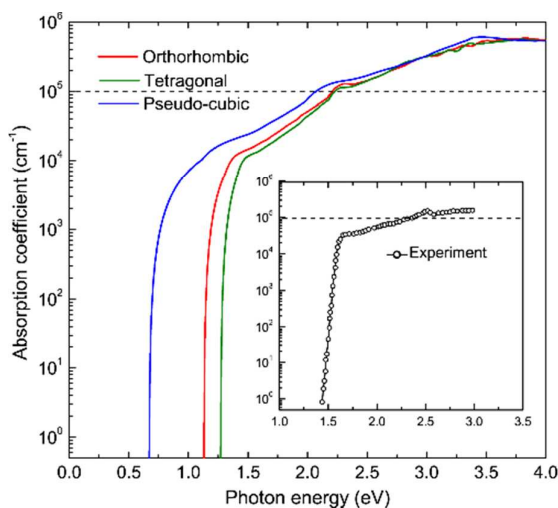


Fig. 1. Calculated absorption coefficient of three phases averaged over nonequivalent directions. The inset also shows the experimental result[11].

### 3.4. Thermal movements of organic base and photovoltaic performance

As discussed above, the thermal movement (or orientational disorder) effect of the organic base is approximated in our theoretical calculations. In this section, we briefly argued the thermal movement effect on the transport and optical properties of $CH_3NH_3PbI_3$.

It should be noticed that both the transport and optical properties are mainly determined by the near-edge electronic properties (see Supplementary materials). Therefore, the organic base is not expected to have direct influences on those properties, since the organic base only contributes to the states with much lower energy. Nevertheless, the thermal movement of organic base can change the inorganic Pb-I framework, i.e., the calculated Pb-I bond-lengths are 3.18, 3.22, and 3.14 Å for orthorhombic, tetragonal, and pseudo-cubic structures, respectively. In other words, the essential structural difference between the three phases is the deformation of the Pb-I octahedra induced by organic base. Interestingly, the structural difference can change the near-edge band structures substantially (see Fig. 2), because both the band-edge valence and conduction states are from the Pb-I framework.

As shown in Table I, the thermal movement of organic base has a significant influence on the effective masses for both the electrons and holes. As the Pb-I bond length decreases from the tetragonal (i.e., 3.22 Å) to the orthorhombic (i.e., 3.18 Å) and to the pseudo-cubic phase (i.e., 3.14 Å), the interaction between Pb cations and I anions increases, resulting in much wider band widths (see Fig. 2) and thus smaller effective masses. As a result, the pseudo-cubic phase has the highest carrier mobilities among the three phases. Another important influence of organic base on the bandgap is also ascribed to the Pb-I bond length. As the Pb-I bond length decreases, the enhanced Pb-I interaction and thus the wider band width lead to smaller bandgap. Whereas the bandgap of pseudo-cubic phase ($E_g = 0.67$ eV) is too small for a photon absorber, the bandgap of the tetragonal phase ($E_g = 1.27$ eV) is more ideal for photovoltaic devices. Both the transport and optical properties can be sensitively influenced by the thermal movement effect of the organic base via an indirect way.
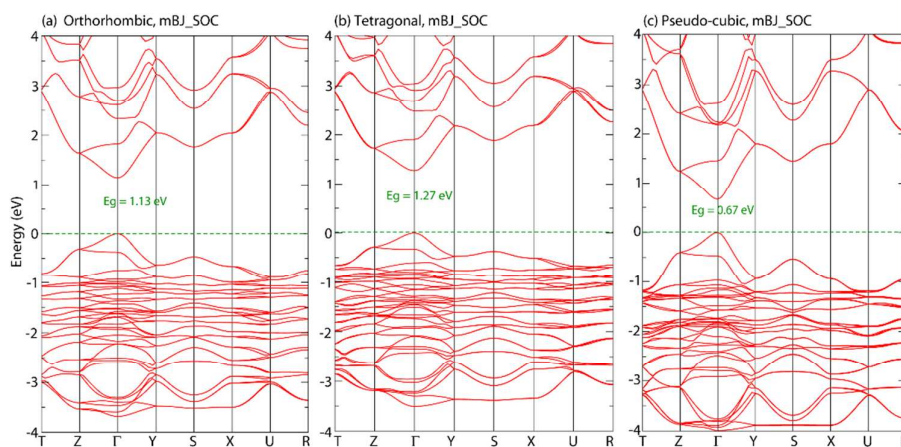


Fig. 2. Band structures of (a) orthorhombic, (b) tetragonal, and (c) cubic phases using mBJ potential. The spin-orbit coupling effect is considered in the calculation. The dispersion curves are along directions of T(-½,0,½) → Z(0,0, ½) → Γ(0,0,0) → Y(-½,0,0) → S(-½,½,0) → X(0, ½,0) → U(0, ½, ½) → R(½,½,½). The VBMs are set to be zero.

## 4. Conclusions

To gain insights to the superior photovoltaic material of $CH_3NH_3PbI_3$, we carried out theoretical investigations on the carrier transport and the optical properties using the first-principles approaches. We found that the theoretically predicted carrier mobilities are as high as $(7 \sim 30) \times 10^3$ and $(1.5 \sim 5.5) \times 10^3$ cm$^2$/V·s for band-edge electron and hole, respectively. The high carrier mobilities are ascribed to the small effective masses at band-edge states, due to the strong anti-bonding interaction between Iodine and Lead. Besides, this material has superior optical properties, i.e., it has sharp photon absorption edge and high absorption coefficient around $10^5$ cm$^{-1}$. The

unique performance of $CH_3NH_3PbI_3$ gives rise to the high efficiency of photovoltaic devices.

The influence of thermal movement of organic base on the photovoltaic performance is rather complicated. The direct consequence of this effect is to the crystal structural properties, leading to different deformations to the Pb-I framework. Because the near-edge states depends on the Pb-I interaction, both the carrier transport and optical properties are sensitively influenced by the thermal movement effect of the organic base via an indirect way. Whereas the carrier transport properties are improved for high-temperature pseudo-cubic phase, the band gap is ideal for the mid-temperature tetragonal phase as a photon absorber. We argued that the optimal performance of a practical solar cell can be achieved by considering the detailed balance between the carrier transport and optical properties via the temperature effect.

## Reference

1    R. W. G. Wyckoff, Am. J. Sci., 1928, **16**, 349-359.

2    Y. Chiba, A. Islam, Y. Watanabe, R. Komiya, N. Koide and L. Han, Jpn. J. Appl. Phys., 2006, **45**, 638-640.

3    L. Han, A. Islam, H. Chen, C. Malapaka, B. Chiranjeevi, S. Zhang, X. Yang and M. Yanagida, Energy Environ. Sci., 2012, **5**, 6057-6060.

4    J. Burschka, N. Pellet, S. J. Moon, R. Humphry-Baker, P. Gao, M. K. Nazeeruddin and M. Gratzel, Nature, 2013, **499**, 316-319.

5    M. Liu, M. B. Johnston and H. J. Snaith, Nature, 2013, **501**, 395-398.

6    S. D. Stranks, G. E. Eperon, G. Grancini, C. Menelaou, M. J. Alcocer, T. Leijtens, L. M. Herz, A. Petrozza and H. J. Snaith, Science, 2013, **342**, 341-344.

7    G. Xing, N. Mathews, S. Sun, S. S. Lim, Y. M. Lam, M. Gratzel, S. Mhaisalkar and T. C. Sum, Science, 2013, **342**, 344-347.

8    T. C. Sum and N. Mathews, Energy Environ. Sci., 2014, **7**, 2518-2534.

9    M. A. Green, A. Ho-Baillie and H. J. Snaith, Nature Photon., 2014, **8**, 506-514.

10    P. Jackson, D. Hariskos, E. Lotter, S. Paetel, R. Wuerz, R. Menner, W. Wischmann and M. Powalla, Prog. Photovoltaics, 2011, **19**, 894-897.

11    S. De Wolf, J. Holovsky, S. J. Moon, P. Löper, B. Niesen, M. Ledinsky, F. J. Haug, J. H. Yum and C. Ballif, J. Phys. Chem. Lett., 2014, **5**, 1035-1039.

12    J. M. Frost, K. T. Butler, F. Brivio, C. H. Hendon, M. van Schilfgaarde and A. Walsh, Nano Lett., 2014, 14, 2584-2590.

13    W. J. Yin, T. Shi and Y. Yan, Appl. Phys. Lett., 2014, **104**, 063903.

14    C. C. Stoumpos, C. D. Malliakas and M. G. Kanatzidis, Inorg. Chem., 2013, **52**, 9019-9038.

15    S. Sun, T. Salim, N. Mathews, M. Duchamp, C. Boothroyd, G. Xing, T. C. Sum and Y. M. Lam, Energy Environ. Sci., 2013, **7**, 399-407.

16    W. Shockley and H. J. Queisser, J. Appl. Phys., 1961, **32**, 510.

17    J. Bardeen and W. Shockley, Phys. Rev. 1950, **80**, 72-80.

18    P. E. Blochl, Phys. Rev. B, 1994, **50**, 17953-17979.

19    G. Kresse, Phys. Rev. B, 1999, **59**, 1758-1775.

20    G. Kresse, Phys. Rev. B, 1996, **54**, 11169-11186.

21    G. Kresse and J. Furthmüller, Comp. Mater. Sci., 1996, **6**, 15-50.

22    H. J. Monkhorst and J. D. Pack, Phys. Rev .B, 1976, **13**, 5188-5192.

23    M. Dion, H. Rydberg, E. Schroder, D. C. Langreth and B. I. Lundqvist, Phys. Rev .Lett., 2004, **92**, 246401.

24    J. Klimes, D. R. Bowler and A. Michaelides, Phys. Rev. B, 2011, **83**, 195131.

25  J. P. Perdew, K. Burke and M. Ernzerhof, Phys. Rev. Lett., 1996, **77**, 3865-3868.

26  A. D. Becke and E. R. Johnson, J. Chem. Phys., 2006, **124**, 221101.

27  F. Tran and P. Blaha, Phys. Rev. Lett., 2009, **102**, 226401.

28  D. Koller, F. Tran and P. Blaha, Phys. Rev. B, 2011, **83**, 195134.

29  D. Koller, F. Tran and P. Blaha, Phys. Rev. B, 2012, **85**, 155109.

30  We notice that some matrix elements $[\hat{\mathbf{H}}, \hat{\mathbf{r}}]$ are neglected so far when using the mBJ potential for the dielectric function calculation in the VASP (version 5.3).

31  P. Blaha, K. Schwarz, G. Madsen, D. Kvasnicka and J. Luitz, WIEN2k, An Augmented Plane Wave + Local Orbitals Program for Calculating Crystal Properties (Karlheinz Schwarz, Techn. Universität Wien, Austria), 2001.

32  T. Baikie, Y. Fang, J. M. Kadro, M. Schreyer, F. Wei, S. G. Mhaisalkar, M. Graetzel and T. J. White, J. Mater. Chem. A, 2013, **1**, 5628-5641.

33  A. Franceschetti, S. H. Wei and A. Zunger, Phys. Rev. B, 1994, **50**, 17797-17801.

34  S. H. Wei and A. Zunger, Phys. Rev. B, 1999, **60**, 5404-5411.

35  Y. H. Li, X. G. Gong and S. H. Wei, Appl. Phys. Lett., 2006, 88, 042104.

36  Y. He and G. Galli, Chem. Mater., 2014, **26**, 5394-5400.

37  Y. I. Ravich, B. A. Efimova and I. A. Smirnov, Semiconducting Lead Chalcogenides; Plenum Press: New York, 1970, 85–216

38  M. Long, L. Tang, D. Wang, Y. Li and Z. Shuai, ACS Nano, 2011, **5**, 2593-2600.